Journal of Nuclear Materials 524 (2019) 60–66

Contents lists available at ScienceDirect

Journal of Nuclear Materials

journal homepage: www.elsevier.com/locate/jnucmat

Irradiation effects of medium-entropy alloy NiCoCr with and without pre-indentation

Chenyang Lu [a, *], Tai-Ni Yang [a], Ke Jin [b], Gihan Velisa [b], Pengyuan Xiu [a], Qing Peng [a], Fei Gao [a], Yanwen Zhang [b, c], Hongbin Bei [b], William J. Weber [b, c], Lumin Wang [a, d, **]

[a] Department of Nuclear Engineering and Radiological Sciences, University of Michigan, Ann Arbor, MI, 48109, USA
[b] Materials Science and Technology Division, Oak Ridge National Laboratory, Oak Ridge, TN, 37831, USA
[c] Department of Materials Science and Engineering, University of Tennessee, Knoxville, TN, 37996, USA
[d] Department of Materials Science and Engineering, University of Michigan, Ann Arbor, MI, 48109, USA

GRAPHICAL ABSTRACT

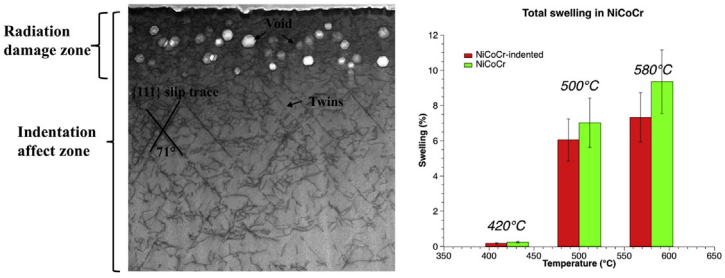

ARTICLE INFO

Article history:
Received 28 December 2018
Received in revised form
8 June 2019
Accepted 10 June 2019
Available online 21 June 2019

Keywords:
Medium entropy alloy
Void swelling
Structural complexity
Ion beam irradiation

ABSTRACT

Medium entropy alloy NiCoCr draws great attention due to its excellent strength-ductility trade-off mechanical behavior. Its irradiation behavior at elevated temperatures has been investigated using ion beam irradiation in a temperature range of 420–580°Cand transmission electron microscopy. Irradiation induced stacking fault tetrahedra were only observed at 420 °C. With increasing irradiation temperature, all stacking fault tetrahedra vanished, while the size of voids and dislocation loops increased significantly. Nanoindentation-induced structural complexities, including dislocations, stacking faults and twins helped to reduce void swelling. However, at the elevated temperatures, NiCoCr is still much more susceptible to void swelling compared to high entropy alloys such as NiCoFeCrMn and NiCoFeCrPd.
Published by Elsevier B.V.

1. Introduction

High entropy alloys (HEAs), normally comprising five or more multiple principal components, have currently generated considerable interests in the materials science community due to their multifunctional properties derived from the complex combinations of compositional elements. One of the extensively investigated face-centered-cubic (fcc) structured HEAs, equiatomic NiCoFeCrMn, displays excellent strength-ductility trade-off due to the unusual behavior in twining and stacking fault at ambient and cryogenic temperatures [1–5]. Furthermore, another amazing

* Corresponding author.
** Corresponding author. Department of Nuclear Engineering and Radiological Sciences, University of Michigan, Ann Arbor, MI, 48109, USA.
E-mail addresses: chenylu@umich.edu (C. Lu), lmwang@umich.edu (L. Wang).

https://doi.org/10.1016/j.jnucmat.2019.06.020
0022-3115/Published by Elsevier B.V.

feature of NiCoFeCrMn is its superior radiation tolerance demonstrated by several recent studies [6–9]. Due to its promising mechanical properties and excellent radiation resistant behavior, NiCoFeCrMn, as well as other HEAs, has been proposed as a candidate structural material in the advanced reactor systems [8,10–12].

Interestingly, recent work has shown that increasing the number of component elements in alloys is not necessary to achieve outstanding mechanical properties [13]. Thus, a more general family of alloys, single-phase concentrated solid-solution alloys (SP-CASs), has been gradually explored. One of the remarkable results is the medium entropy alloy (MEA) equiatomic NiCoCr, which exhibits outstanding yield strength and ultimate tensile strength, companying with an exceptional ductility [13]. The MEA NiCoCr shows even better mechanical properties than the HEA NiCoFeCrMn. Deformation mechanisms of NiCoCr have been extensively investigated by previous studies for the extraordinary mechanical behaviors, which is attributed to its capacity for twinning-controlled deformation [14–16]. Because of the intriguing properties and unique deformation mechanism, it is very interesting to systematically study the radiation behavior of NiCoCr. Recently, NiCorCr has been experimentally studied in response to Ni ion irradiations at room temperature by ion channeling technique, and the results demonstrate a comparable radiation resistance to NiCoFeCr and much better radiation resistance than pure Ni and NiCo [17]. However, the irradiation response of NiCoCr at elevated temperatures is scarce.

In previous studies, we systematically investigated the effects of compositional complexity on radiation response in SP-CSAs by tuning the number, species, and concentration of alloying elements in a wide range of composition without changing crystal structures (fcc or bcc) [6,18,19]. These studies clearly demonstrate that modifying alloy compositional complexity will enable to control defect dynamics at the early stage of radiation damage and to ultimately enhance radiation tolerance at the later stage under extreme radiation conditions. On the other hand, structural complexity is also a very important aspect to design radiation tolerant material. In this work, we aim to examine the lower boundary requirement of the structural complexity by reducing the number of alloying species to three, i.e. NiCoCr as a model material for this investigation. Several aspects of structural complexity, high-density dislocation pile-ups, stacking faults, and twin boundaries, have been introduced into the NiCoCr alloys through nanoindentation. We focus on a particular issue that how these pre-existing structure complexities affect the void formation and accumulation in MEA NiCoCr.

2. Experimental

The equiatomic NiCoCr alloy used in this study was synthesized by arc-melting a mixture of high-purity raw elements [20]. Prior to irradiation, nanoindentation was intentionally conducted to deform the sample surface. The nanoindentation tests were performed on a Nanoindenter XP at a constant $\dot{P}/P = 0.05\ s^{-1}$ using a spherical sapphire indenter with a diameter of 200 μm. The indentation depth of 2 μm was set for the sample, which resulted in residual depths of ~1.7 μm after the recovery of elastic displacement. The indented samples were irradiated with 3 MeV Ni^{2+} ions to a fluence of $5 \times 10^{16}/cm^2$ at 420 °C, 500 °C and 580 °C. All the irradiations were performed at Ion Beam Materials Laboratory (IBML) at the University of Tennessee, Knoxville [21]. A defocused beam was wobbled to achieve uniform irradiation, with scanning frequencies of 517 and 64 Hz for the horizontal and vertical direction, respectively. The irradiation period for each setup was about 5 h and the temperature fluctuation was controlled in ±5 °C. The corresponding displacements per atom (dpa) and implanted Ni ion concentration were calculated using Stopping Range of Ions in Matter (SRIM) 2013 code in Kinchin-Pease mode with a displacement threshold energy of 40 eV, as shown in Fig. 1. The peak dose is about ~52 dpa. The cross-sectional TEM samples were prepared by focused ion beam (FIB) equipped on a FEI Helios Nanolab dualbeam scanning electron microscopy (SEM), followed by flash polishing technique [22] to remove the FIB-induced damages. The schematic of indentation, irradiation and FIB foil position is shown in Fig. 2. A double Cs-corrected S/TEM JEOL 3100R05 was used for both TEM and STEM imaging operated at 300 keV. Voids were characterized by TEM with under-focused condition in bright field (BF) mode. Other irradiation- and deformation-induced features were all characterized by the on-zone scanning TEM (STEM) with a BF mode. STEM images were taken with an inner angle of 59 mrad and camera length of 15 cm.

3. Results and discussion

Fig. 3 shows the cross-sectional BF images of un-indented and pre-indented NiCoCr MEAs irradiated at three different temperatures. The ion irradiation direction is from left to right as shown in the images. Voids were shown in all the investigated samples. Fig. 4(a) shows the depth distribution of the average void diameter in un-indented and pre-indented NiCoCr after three temperature irradiations. Apparently, the void size increased significantly with increasing the irradiation temperature from 420 to 580 °C. Fig. 4(b) shows the depth distribution of void density in NiCoCr. In both un-indented and indented NiCoCr irradiated at 420 °C, the voids are distributed near the sample surface and in a region beyond the calculated damage peak of ~900 nm. With increasing the irradiation temperature, the void densities dropped notably because of the coalescence and growth of the voids. On the other hand, the void sizes are clearly smaller in indented NiCoCr alloys than in un-indented NiCoCr alloys under all the irradiation temperatures as shown in Figs. 3 and 4(a). The depth distribution of void swelling and the total swelling (the depth was selected as 1800 nm to be consistent with the previous studies [6]) are calculated based on the TEM observations according to the formula detailed in Ref. [23]. The results are shown in Fig. 4(c) and (d), separately. Obviously, the indented NiCoCr alloys exhibit better swelling resistance than un-indented NiCoCr alloys, indicating that the indentation-induced structural complexities can suppress the void growth in NiCoCr alloys. It is worth noting that, although the void distribution peak

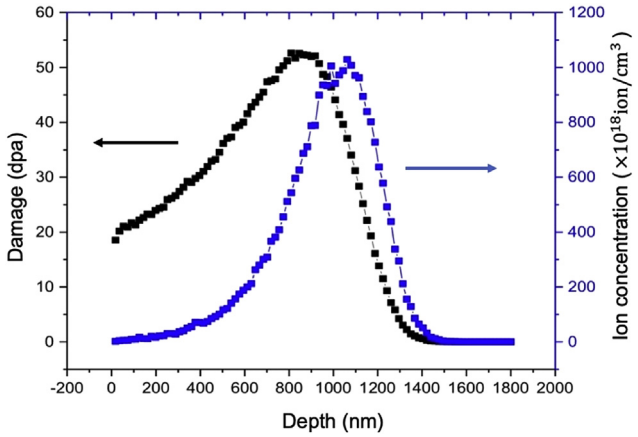

Fig. 1. Depth profiles of displacement per atom (dpa) and induced Ni ion concentration predicted by SRIM code for NiCoCr irradiated with 3 MeV Ni^{2+} ions to a fluence of $5 \times 10^{16}\ cm^{-2}$.

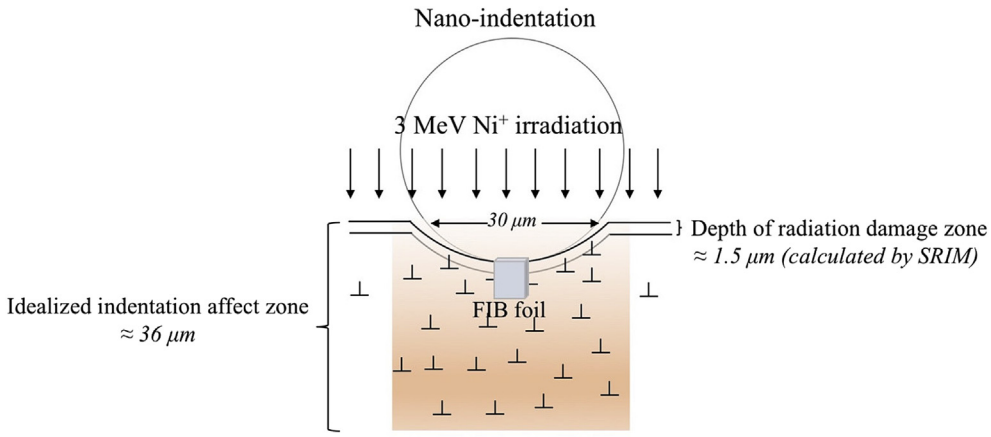

Fig. 2. Schematic of indentation, irradiation and FIB foil position in indented NiCoCr.

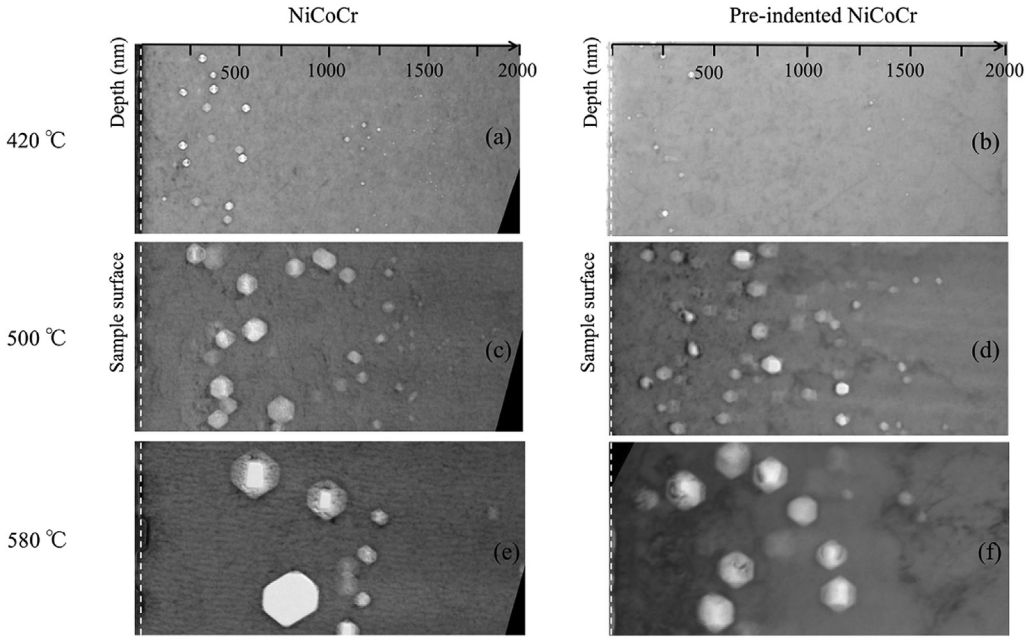

Fig. 3. Cross-sectional BF TEM images showing void distributions in (a) (c) (e) un-indented NiCoCr and (b) (d) (f) pre-indented NiCoCr irradiated with 3 MeV Ni^{2+} ions to 5×10^{16} cm^{-2} at (a) (b) 420 °C, (c) (d) 500 °C and (e) (f) 580 °C. The ions enter the specimen from the left of the images.

(void density) is around 1400 nm depth, the average size of voids and local swelling peak is actually around 800–900 nm as shown in Fig. 4(a) and (c). It indicates that most of survived vacancies stayed in the peak damage region and coalesced to form into large voids. Only a small amount of vacancies migrates into the deeper region to form small voids. A similar void distribution has been reported in authors' previous study [6]. Furthermore, as can be seen in Figs. 3(a) and 4(b), the void separation in depth is significantly in NiCoCr irradiated at 420 °C. It can be explained by the injected interstitial mechanism. The void swelling was suppressed at the high Ni ion concentration region and void denuded zone was observed as shown in Fig. 3(a). With increasing the irradiation temperature, the migration rate of interstitials increases. It results that the injected interstitials can quickly migrate away. It would either escape toward the surface or toward a much deeper region through 1 dimensional migration motion [18]. It can explain the reason that why there are no denuded zones in NiCoCr irradiated at 500 °C and 580 °C.

Although NiCoCr exhibits a comparable radiation resistance to NiCoFeCr, and much greater suppression of accumulated damage than NiFe and NiCoFe after Ni ion irradiation at room temperature [17], the swelling behavior of NiCoCr after irradiations at elevated temperatures is very poor. The previous and current results of the total swelling value of pure Ni and nickel-containing SP-CSAs irradiated by 3 MeV Ni^{2+} ions to the fluence of $5 \times 10^{16}/cm^2$ at different temperatures [6,24,25] are summarized in Table 1 for comparison. Obviously, NiCoCr has a very poor swelling resistance behavior among all the SP-CSAs. The total swelling value in NiCoCr exhibits more than one order magnitude higher than other SP-CSAs, even worse than binary alloy NiFe. It indicates that similar to the mechanical properties, simply increasing the number of component elements is also not always the best way to enhance the swelling behavior in SP-CSAs. The species of mixing elements sometimes plays a dominant role in defect formation and accumulation as concluded in previous studies [10,18]. Furthermore, NiCoFe has much lower swelling than NiCoCr, indicating that

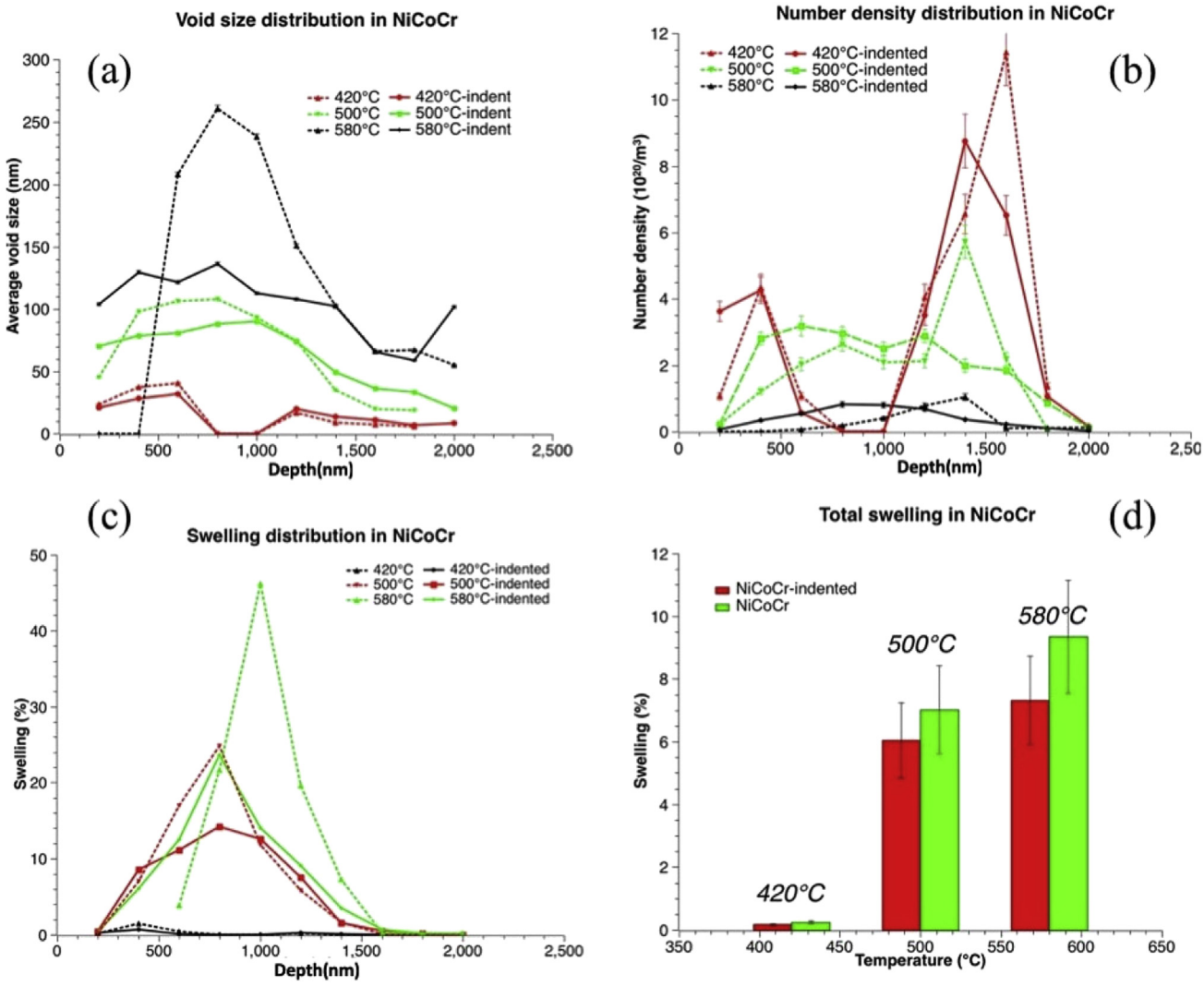

Fig. 4. Depth distributions of (a) average void diameter, (b) void density and (c) swelling, and (d) total swelling of un-indented and indented NiCoCr irradiated with 3 MeV Ni^{2+} ions to a fluence of 5×10^{16} cm^{-2} at different temperatures.

Table 1
Summary of total swelling value in 3 MeV Ni^{2+} irradiated pure Ni and nickel-contained SP-CSAs in the region of 0-1800 nm from surface, with irradiation temperature as 420, 500, 580°C [6,24,25].

Temperature	Ni	NiFe	NiCoFe	NiCoCr	NiCoFeCrMn	NiCoFeCrPd
420°C	/	/	/	~0.24%	~0.02% [24]	~0.003% [24]
500°C	~9.4%[6]	~0.45%[6]	~0.15%[6]	~7.01%	~0.1% [6,24]	~0.1% [24]
580°C	/	/	/	~9.34%	~0.37% [24]	~0.3% [24,25]

alloying with Fe is much more effective in suppressing void swelling than alloying with Cr. Further increasing the element number to five, two HEAs NiCoFeCrMn and NiCoFeCrPd have shown significant improvement of swelling resistance compared to their mutual ternary alloys NiCoCr, suggests that Fe/Mn and Fe/Pd elements can compensate the negative influence of Cr element. Therefore, choosing the element species and the number of elements plays a synergistic effect on radiation behavior in SP-CSAs. Balancing the two competing aspects is very important to increase the compositional complexity in SP-CSAs, subsequently providing the guidance to design the new type of radiation resistant materials.

To understand the differences of swelling behavior in un-indented NiCoCr and indented NiCoCr, it is necessary to investigate the indentation- and irradiation-induced structural changes in alloy matrix. Fig. 5(a–c) show the panoramic cross-sectional STEM-BF images of indented NiCoCr after 420 °C, 500 °C and 580 °C irradiations, respectively. The images were taken near the [110] zone axis. On-zone STEM-BF characterization method can maximize the visibility of all the indentation- and irradiation-induced features because of the multi-beam diffraction condition achieved [26]. Radiation damage zone has been observed as a dark band stretched from the sample surface to an extended depth in the images. Fig. 5(d–f) are the enlarged images of the damaged zone from the colored rectangles in Fig. 5(a–c), respectively. As shown in Fig. 5(d–f), the high densities of dislocations loops are observed in

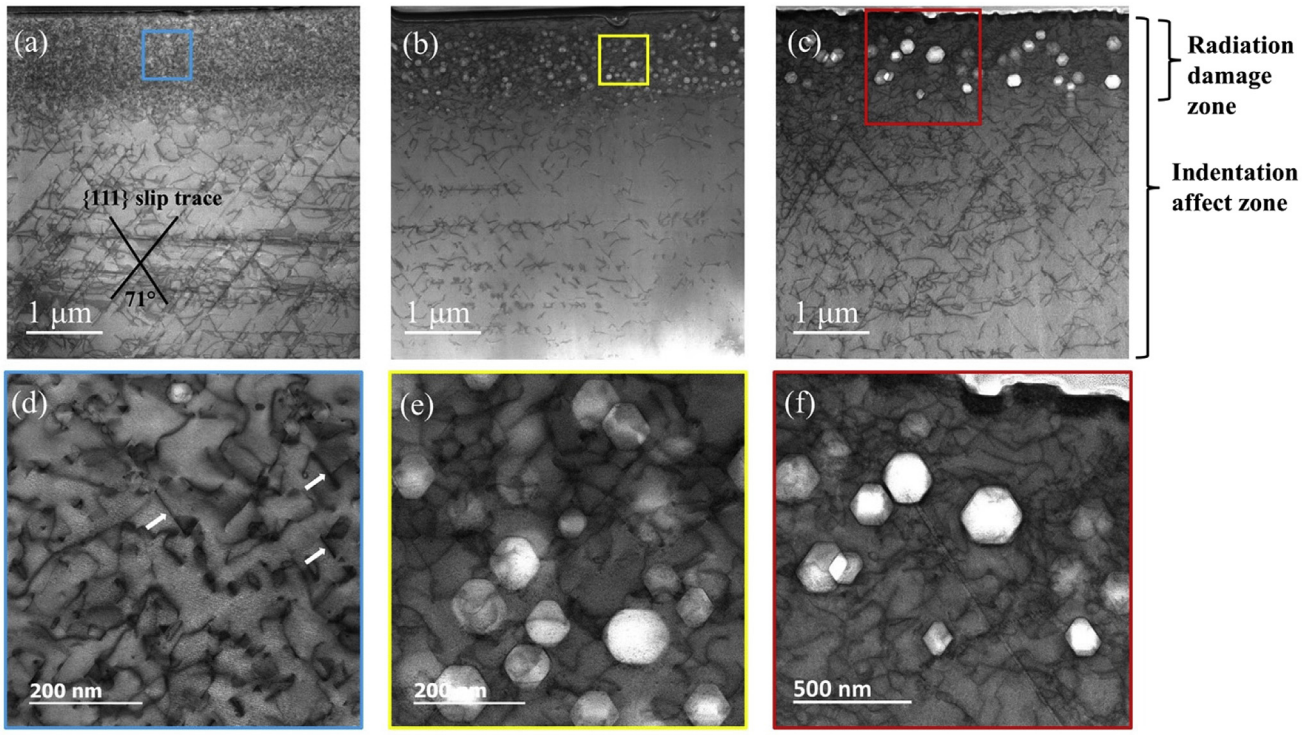

Fig. 5. On-zone cross-sectional STEM-BF images of indented NiCoCr irradiated at (a) 420 °C, (b) 500 °C and (c) 580 °C. Enlarged images of damaged zone from the colored rectangles in (a) (b) (c) are shown in (d) (e) (f), respectively.

all NiCoCr alloys. Based on the previous studies in SP-CSAs, the dislocation loops are condensed by the survived interstitials from ion irradiations. Clearly, the loop size increases significantly with increasing irradiation temperature, which is consistent with Yang et al. study in $Al_{0.1}$CoCrFeNi to 31 dpa at 250–650 °C [9]. Because of the large size of dislocation loops, it is unlikely to statistically determine the loop distribution in a certain depth with a specific irradiation dose. Instead, all the loops distributed in the whole damage region were counted for statistics. The loop sizes were determined by measuring the longest axis of the loops. NiCoCr irradiated at 420 °C shows the smallest loop size with an average diameter of 47.0 ± 2.4 nm, and the highest loop density of $2.7 \pm 0.2 \times 10^{21}/m^3$. NiCoCr irradiated at 500 °C has an average loop diameter of 96 ± 2 nm and a loop density of $1.0 \pm 0.1 \times 10^{21}/m^3$. NiCoCr irradiated at 580 °C has a much larger loop size of 157±1 nm and relatively low loop density of $3.6 \pm 0.3 \times 10^{20}/m^3$. It is well known that the dislocation loops in nickel-containing SP-CSAs are usually in consist of a mixture of perfect $\frac{1}{2}<110>$ and faulted $\frac{1}{3}<111>$ loops [7]. The white marks in Fig. 5(d) indicate the typical edge-on faulted loops in NiCoCr according to the geometry feature. With increasing irradiation temperatures, the loops grew very fast through the fast migration of the single defects and the coalesce of the interstitial clusters. Most of the loops were all untangled and formed into network dislocations including dislocation lines and large dislocation loops in NiCoCr after irradiated at 580 °C. Compared to other nickel-containing SP-CSAs irradiated at 500 °C, the size of dislocation loops in NiCoCr is slightly larger than in NiFe, much larger than in NiCoFe, NiCoFeCr and NiCoFeCrMn. The density of the dislocation loops in NiCoCr is comparable to NiFe, but much lower than others [7].

A great number of tiny stacking-fault tetrahedra (SFTs) were also observed in the NiCoCr irradiated at 420 °C. The number density of SFTs is $2.0 \pm 0.2 \times 10^{22}/m^3$, and the average size of SFTs is 8.0 ± 0.5 nm. However, no SFTs can be found in NiCoCr irradiated at higher temperatures. More interestingly, all the SFTs only distributed around the large voids. The detailed characterization of the positional relation between SFTs and voids is shown in Fig. 6(a). This present finding is of interest for understanding the transformation process from SFTs to voids. The direct evidence shows that the voids are preferred to nucleate at the sites of SFTs. Furthermore, the SFTs are all disappeared in NiCoCr irradiated at higher temperatures. The void swelling value has a large increment from 420 °C to 500 °C as shown in Fig. 4(d). It is reasonable to believe that the growth of the voids is achieved by absorbing the vacancies in the SFTs. At 420 °C, part of the survived vacancies condensed into SFTs and rests condensed into voids. At 500 °C, all the survived vacancies were all formed into voids and contributed to the large swelling in NiCoCr. It is known that the migration of SFT is very hard because of its stable tetrahedron structure. Therefore, it is speculated that small SFTs could become thermally unstable and disassemble into small vacancy clusters at high temperatures. As a consequence, vacancy clusters migrate and agglomerate to form large voids. However, the detailed disassembly of the SFTs, as well as the formation of voids and the growth of voids by absorbing vacancy clusters, are not clear. Dynamic observation by ion-beam in-situ TEM and computation simulation are needed to provide more details on this transformation process in future studies.

As shown in Fig. 5(a–c), indentation-induced structures are observed in the indentation affect zone, which is under the radiation damage zone as shown in the right side of Fig. 5(c). Typical dislocation glide occurs on several different {111} planes. To be noted, the dislocation densities in the indentation affected zone have no significant changes with increasing irradiation temperatures from 420 °C to 580 °C, indicating that the deformation structures were not annealed under this temperature regime. In addition to dislocation slips, high density of stacking faults (SFs) was also introduced by the nanoindentation. Fig. 6(b) reveals the presence of extended SFs on different {111} planes that intersect

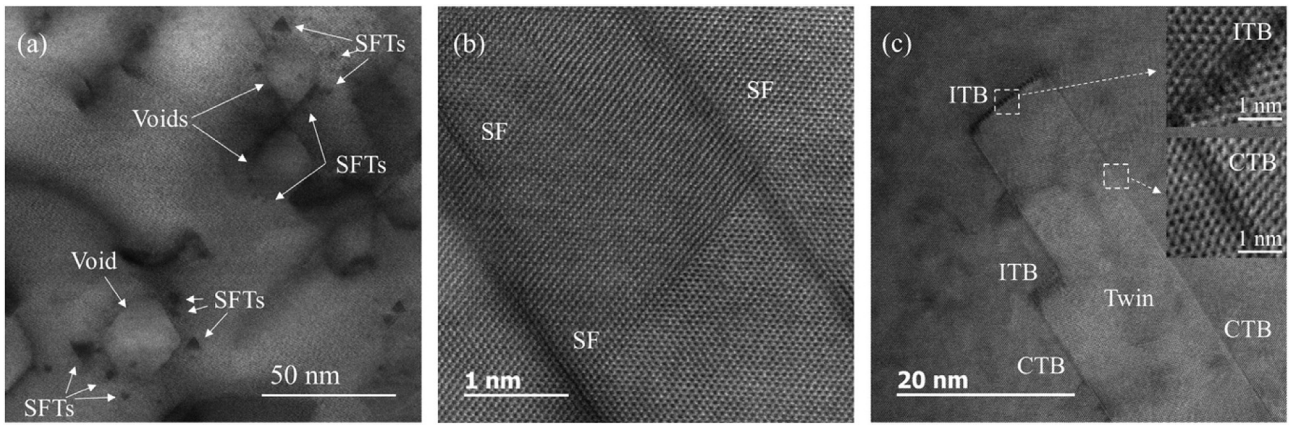

Fig. 6. (a) STEM-BF image showing the voids and SFTs in NiCoCr irradiated at 420 °C. (b) STEM-BF image showing the SFs introduced by nanoindentation in NiCoCr. (c) STEM-BF image showing the twin boundaries introduced by nanoindentation in NiCoCr.

each other. Moreover, typical twins were also observed as shown in Fig. 6(c). Two types of twin boundaries were marked: $\Sigma_3\{111\}$ coherent twin boundaries (CTB) and $\Sigma_3\{112\}$ incoherent twin boundaries (ITB). It is known that the formation of extended SFs plays key roles in the formation of twins. There are extensive studies [14,15] to investigate the deformation mechanisms, as well as the relations between SFs and twins in NiCoCr, which is not discussed in details in this study. However, this result is in good agreement with previous studies that NiCoCr has a very low stacking fault energy and very high propensity for twining under low-level deformation [14,15].

It is worth noting that, in a previous study [25], nanoindentation enhanced void swelling in high entropy alloy NiCoFeCrPd. The contradictory observations from NiCoCr and NiCoFeCrPd can be explained by the following three reasons. First, nanoindentation can introduce much higher density of defect sinks in NiCoCr than in NiCoFeCrPd. Indentation induced dislocation density in NiCoCr is $1.8 \times 10^{14}/m^2$ by Ham's method, which is about three times higher than dislocation density in NiCoFeCrPd [14,25]. Furthermore, the incoherent edge of twin boundaries may act as extra defect sinks in indented NiCoCr, which was not observed in indented NiCoFeCrPd. Second, swelling behavior affected by the net bias or vacancy supersaturation has been studied by Mansur and other researchers [27–29]. A point defect partitioning factor Q for either vacancies or interstitials is described as below:

$$Q = Z_d N_d / 4\pi r N_c Z_c \quad (1)$$

in which, Z_d *and* Z_c are sink capture efficiency for dislocations and cavities, N_d *and* N_c are the concentration for dislocations and cavities, r is cavity radius. On the assumption that Z_d/Z_c is near unity the quantity $Q' = N_d/4\pi r N_c$ is approximately equal to Q. The parameter Q measures the importance of point defect loss to dislocations relative to loss to cavities. When $Q>>1$, it is dislocation dominant regime; When $Q<<1$, it is cavity dominant regime. According to this equation, $Q_{NiCoFeCrPd}$ of indented NiCoFeCrPd is about 0.31, given by the dislocation density of $0.59 \times 10^{14}/m^2$, the average void size of 31 nm and the void density of $4.9 \times 10^{20}/m^3$ [25]. Therefore, the sink strength of indented NiCoFeCrPd falls to the cavity dominant regime. The point defect prefers to loss to cavities, leading to an enhanced void swelling in NiCoFeCrPd with increasing pre-existing dislocations. On the other hand, Q_{NiCoCr} of indented NiCoCr is about 6, which is much higher than 1. It leads the sink strength of indented NiCoCr falls to the dislocation dominant regime. Therefore, the pre-existing dislocations in indented NiCoCr suppress void swelling. The equation can explain the different effects of pre-existing dislocations on swelling behavior in NiCoCr and NiCoFeCrPd. Third, it is reasonable to assume that vacancies can migrate much faster in NiCoCr than in NiCoFeCrPd as evidenced by the formation of much large voids. Therefore, vacancies can reach defect sinks much easier for annihilation than in NiCoFeCrPd. It is generally believed that the structural complexities, such as grain boundaries, dislocations, and the interfaces between the matrix and precipitates, can act as sinks for absorbing both vacancies and interstitials, although some of these sinks are biased for interstitials [30,31]. Apparently, indentation-induced microstructural features observed in this study have effectively reduced void swelling in NiCoCr as shown in Figs. 3 and 4(d).

4. Conclusion

In conclusion, MEA NiCoCr was irradiated by 3 MeV Ni^{2+} ions to study its irradiation responses in a temperature range between 420 and 580 °C. It was found that, although the alloy has excellent mechanical properties and good radiation tolerance at the room temperature, it is much more susceptible to void swelling while irradiated at elevated temperatures as compared with the other SP-CSAs. The species of mixing elements plays a dominant role in defect formation and accumulation in NiCoCr. The void and dislocation densities decrease but their sizes increase significantly with increasing irradiation temperature. Furthermore, indentation-induced structural complexities, including dislocation slips, SFs, and twin boundaries, have effectively decreased the amount of void swelling in NiCoCr due to enhanced annihilation of vacancies at these microstructural features.

Acknowledgement

This work was supported as part of the Energy Dissipation to Defect Evolution (EDDE), an Energy Frontier Research Center funded by the US Department of Energy, Office of Science, Basic Energy Sciences under contract number DE-AC05-00OR22725. Ion beam work was performed at the UT–ORNL Ion Beam Materials Laboratory located on the campus of the University of Tennessee–Knoxville. Microstructure characterizations were conducted in the Michigan Center for Material Characterization of the University of Michigan.

References

[1] B. Cantor, I.T.H. Chang, P. Knight, A.J.B. Vincent, Mater. Sci. Eng. A 375–377 (2004) 213–218.
[2] J.W. Yeh, S.K. Chen, S.J. Lin, J.Y. Gan, T.S. Chin, T.T. Shun, C.H. Tsau, S.Y. Chang, Adv. Eng. Mater. 6 (2004) 299–303.
[3] F. Otto, Y. Yang, H. Bei, E.P. George, Acta Mater. 61 (2013) 2628–2638.
[4] K.G. Pradeep, Y. Deng, Z. Li, D. Raabe, C.C. Tasan, Nature 534 (2016) 227–230.
[5] B. Gludovatz, A. Hohenwarter, D. Catoor, E.H. Chang, E.P. George, R.O. Ritchie, Science 345 (2014) 1153–1158.
[6] C. Lu, L. Niu, N. Chen, K. Jin, T. Yang, P. Xiu, Y. Zhang, F. Gao, H. Bei, S. Shi, M.-R. He, I.M. Robertson, W.J. Weber, L. Wang, Nat. Comms. 7 (2016) 1–8.
[7] C. Lu, T. Yang, K. Jin, N. Gao, P. Xiu, Y. Zhang, F. Gao, H. Bei, W.J. Weber, K. Sun, Y. Dong, L. Wang, Acta Mater. 127 (2017) 98–107.
[8] N.A.P.K. Kumar, C. Li, K.J. Leonard, H. Bei, S.J. Zinkle, Acta Mater. 113 (2016) 230–244.
[9] T. Yang, S. Xia, W. Guo, R. Hu, J.D. Poplawsky, G. Sha, Y. Fang, Z. Yan, C. Wang, C. Li, Y. Zhang, S.J. Zinkle, Y. Wang, Scripta Mater. 144 (2018) 31–35.
[10] Y. Zhang, S. Zhao, W.J. Weber, K. Nordlund, F. Granberg, F. Djurabekova, Curr. Opin. Solid State Mater. Sci. 21 (2017) 221–237.
[11] Y. Zhang, G.M. Stocks, K. Jin, C. Lu, H. Bei, B.C. Sales, L. Wang, L.K. Béland, R.E. Stoller, G.D. Samolyuk, Nat. Comms. 6 (2015).
[12] F. Granberg, K. Nordlund, M.W. Ullah, K. Jin, C. Lu, H. Bei, L.M. Wang, F. Djurabekova, W.J. Weber, Y. Zhang, Phys. Rev. Lett. 116 (2016) 135504–135509.
[13] Z. Wu, H. Bei, G.M. Pharr, E.P. George, Acta Mater. 81 (2014) 428–441.
[14] G. Laplanche, A. Kostka, C. Reinhart, J. Hunfeld, G. Eggeler, E.P. George, Acta Mater. 128 (2017) 292–303.
[15] J. Miao, C.E. Slone, T.M. Smith, C. Niu, H. Bei, M. Ghazisaeidi, G.M. Pharr, M.J. Mills, Acta Mater. 132 (2017) 35–48.
[16] Z. Zhang, H. Sheng, Z. Wang, B. Gludovatz, Z. Zhang, E.P. George, Q. Yu, S.X. Mao, R.O. Ritchie, Nat. Comms. 8 (2017) 14390.
[17] Y. Zhang, K. Jin, H. Xue, C. Lu, R.J. Olsen, L.K. Béland, M.W. Ullah, S. Zhao, H. Bei, D.S. Aidhy, G.D. Samolyuk, L. Wang, M. Caro, A. Caro, G.M. Stocks, B.C. Larson, I.M. Robertson, A.A. Correa, W.J. Weber, J. Mater. Res. 31 (2016) 2363–2375.
[18] T.-N. Yang, C. Lu, G. Velisa, K. Jin, P. Xiu, M.L. Crespillo, Y. Zhang, H. Bei, L. Wang, Acta Mater. 151 (2018) 159–168.
[19] C. Lu, T. Yang, L. Niu, Q. Peng, K. Jin, M.L. Crespillo, G. Velisa, H. Xue, F. Zhang, P. Xiu, Y. Zhang, F. Gao, H. Bei, W.J. Weber, L. Wang, J. Nucl. Mater. 509 (2018) 237–244.
[20] K. Jin, B.C. Sales, G.M. Stocks, G.D. Samolyuk, M. Daene, W.J. Weber, Y. Zhang, H. Bei, Sci. Rep. 6 (2016) 20159.
[21] Y. Zhang, M.L. Crespillo, H. Xue, K. Jin, C.-H. Chen, C.L. Fontana, J.T. Graham, W.J. Weber, Nucl. Instrum. Methods Phys. Res. B 338 (2014) 19–30.
[22] C. Lu, K. Jin, L.K. Béland, F. Zhang, T. Yang, L. Qiao, Y. Zhang, H. Bei, H.M. Christen, R.E. Stoller, L. Wang, Sci. Rep. 6 (2016) 19994.
[23] X. Wang, A.M. Monterrosa, F. Zhang, H. Huang, Q. Yan, Z. Jiao, G.S. Was, L. Wang, J. Nucl. Mater. 462 (2015) 119–125.
[24] T.-N. Yang, C. Lu, G. Velisa, K. Jin, P. Xiu, Y. Zhang, H. Bei, L. Wang, Scripta Mater. 158 (2019) 57–61.
[25] C. Lu, T. Yang, K. Jin, G. Velisa, P. Xiu, M. Song, Q. Peng, F. Gao, Y. Zhang, H. Bei, W.J. Weber, L. Wang, Mater. Res. Lett. 6 (2018) 584–591.
[26] C.M. Parish, K.G. Field, A.G. Certain, J.P. Wharry, J. Mater. Res. 30 (2015) 1–15.
[27] L.K. Mansur, W.A. Coghlan, J. Nucl. Mater. 1 (1983) 119.
[28] N.H. Packan, K. Farrel, J. Nucl. Mater. 677 (1979) 85–86.
[29] L.L. Horton, L.K. Mansur, ASTM STP 870 (1985) 344.
[30] S.J. Zinkle, L.L. Snead, Annu. Rev. Mater. Res. 44 (2014) 241–267.
[31] G.S. Was, Fundamentals of Radiation Materials Science: Metals and Alloys, Springer, 2007.